Characterization of Morphologies of Compatibilized Polypropylene/Polystyrene Blends with Nanoparticles via Nonlinear Rheological Properties from FT-Rheology

ARTICLE *in* MACROMOLECULES · JUNE 2014

Impact Factor: 5.8 · DOI: 10.1021/ma500700e

Macromolecules

Article

pubs.acs.org/Macromolecules

Characterization of Morphologies of Compatibilized Polypropylene/Polystyrene Blends with Nanoparticles via Nonlinear Rheological Properties from FT-Rheology

Reza Salehiyan,[†] Youngjae Yoo,[‡] Woo Jin Choi,[§] and Kyu Hyun*,[†]

[†]School of Chemical and Biomolecular Engineering, Pusan National University, Busan 609-735, Korea

[‡]Division of Advanced Materials, Korea Research Institute of Chemical Technology, Daejeon 305-600, Korea

[§]Chemical Materials Solutions Center, Korea Research Institute of Chemical Technology, Daejeon 305-600, Korea

ABSTRACT: Linear and nonlinear viscoelastic properties under dynamic oscillatory shear flow were used to investigate the effects of compatibilization on polypropylene (PP)/polystyrene (PS) blends. Two different nanoparticles (organo-modified clay and fumed silica) were used at various concentrations. To analyze nonlinear stress under large amplitude oscillatory shear (LAOS) flow, nonlinearity ($I_{3/1}$) was calculated from FT-rheology. To quantify the degree of dispersion of different particles at various concentrations, a new parameter, nonlinear−linear viscoelastic ratio (NLR ≡ normalized nonlinear viscoelasticity/normalized linear viscoelasticity), was used. The relationship was determined between NLR value and PS droplet size in the PP matrix. From the TEM images, clay was located mostly at the interface or partially inside the PS drops, thereby reinforcing the compatibilization effect. Therefore, clay increased the dispersion morphologies of the PP/PS blends. In contrast, fumed silica was located mostly inside the PS droplets, which means the morphologies of PP/PS blends were not improved. Linear viscoelasticities of both PP/PS/clay and PP/PS/silica showed improvements at elevated particle concentrations. NLR values for the PP/PS/Clay blends were larger than 1 (NLR > 1), whereas NLR values for the PP/PS/silica blends were less than 1 (NLR < 1). Therefore, NLR could be classified into two categories depending on morphology. Based on these results, NLR can be used to distinguish between the effects of two different types of nanoparticles on the morphologies of PP/PS blends.

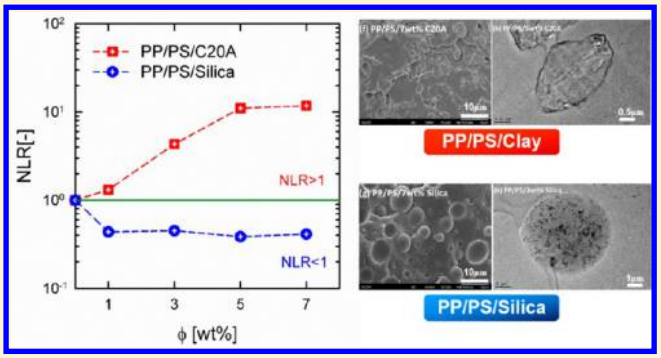

1. INTRODUCTION

Mixing of various polymeric materials has been widely used in recent decades in order to create new materials with desirable characteristics. However, poor compatibility between thermodynamically immiscible polymer blends yields weaker final properties.[1] A few of the governing factors that determine the morphology and final properties of immiscible blends include blend composition, viscosity ratios, processing conditions, and interfacial tension. Hence, one way to control morphology and improve immiscibility of the blends is addition of a well-defined surface-active component known as a compatibilizer.[2−4] When compatibilizers are carefully chosen, compatibilizers can be used as emulsifiers to improve compatibilities in particular blends due to their interfacial activity. Specifically, coalescence, interfacial tensions, dispersion quality, droplet size, and deformations can be controlled by the addition of compatibilizers.[2−10] Improvements in compatibilities largely depend on either the structure, molecular weight, and concentration of compatibilizers or the extent of interfacial reactions in the case of reactive compatibilization.[11] Raghu et al.[12] previously used block copolymers, i.e., styrene−isoprene−styrene (SIS), styrene−butadiene−styrene (SBS), and styrene−butadiene−rubber (SBR), to compatibilize (70/30) polypropylene (PP)/polystyrene (PS) blends. Improved efficiencies of SBS and SBR were obtained over SIS, as the latter caused a drop in viscosity due to its different structure. Slouf et al.[13] determined the efficiency of styrene−ethylene−propylene (SEP) copolymer in compatibilizing PP/PS blends at different compositions and viscosity ratios. Although carefully chosen copolymers have been shown to contribute to the compatibilization of immiscible blends, another category of species known as inorganic fillers has recently drawn the attention of scientists. This group of materials has been shown to be effective in the modification of properties owing to their small scale and high surface area per unit volume. Inorganic fillers become more efficient for compatibilization when organically modified.[44] Organo-modified fillers can modify the morphology of a blend when preferentially accommodated in one of the phases, and they can alter viscosity ratios or migrate to the interface. The latter mechanism reduces interfacial tension, suppresses

Received: April 5, 2014
Revised: June 1, 2014
Published: June 13, 2014

   dx.doi.org/10.1021/ma500700e | *Macromolecules* 2014, 47, 4066−4076

coalescence, and strengthens adhesions between the two phases. Two determinant interactions in filler-filled polymers are (1) filler−filler interactions and (2) polymer−filler interactions. The final structure of fillers inside the polymer, exfoliation or intercalation, highly depends on these interactions. Depending on each structure, final properties will differ.[4,14,15] Ray et al.[4] investigated the effect of C20A (Cloisite 20A, organo-modified montmorillonite) on PP/PS and maleic anhydride-grafted polypropylene/polystyrene (PP-*g*-MA/PS) blends. C20A was found to be located at the interface and reduced interfacial tensions of the blends. However, the compatibilization effect was more efficient in the case of PP-*g*-MA/PS blends. A similar phenomenon was observed when a small amount of organoclay was added to the PBT/PE blends.[16] Wang et al.[15] determined the compatibilization effect of organo-modified montmorillonite (OMMT) on (70/30) PP/PS blends. Interestingly, a more uniform and smaller droplet size was achieved when mixing time increased. Hong et al.[17] compared the effects of chemical affinity and shear stress on the localization of organoclays inside the PBT/PS blend. Clay tactoids were always located inside or at the interface of the more thermodynamically compatible phase, PBT, regardless of mixing sequence, and they migrated toward the more stable phase when shear stress was applied.

Characterization of compatibilized blends via rheological properties has become a major issue.[5,6] Experimental results revealed that blends modified with compatibilizers showed elevated storage modulus $G'(\omega)$, loss modulus $G''(\omega)$, and absolute value of complex viscosity $|\eta^*|(\omega)$ under small-amplitude oscillatory shear (SAOS) within the linear regime depending on the structure and concentration of the compatibilizers used.[5−7] In addition, interfacial tensions as calculated by mathematical models such as the Palierne model,[18] Choi and Schowalter model,[19] or Gramespacher and Meissner model[20] decreased as compatibilizers were added to the blends, which is consistent with reduction of dispersed phase size.[2,18−25] In another report by Li et al., SBS was used as a compatibilizer for a (20/80) PP/PS blend.[25] Elevation of $|\eta^*|(\omega)$ indicated that SBS is efficient in compatibilizing PP/PS blends. Moreover, the most significant improvements in morphology were obtained within the first 2 min of mixing. In a study by Cho et al.,[26] addition of 5 wt % of C20A (Cloisite 20A, organo-modified montmorillonite) brought about a profound increase in compatibility between PP and PS due to its localization at the interface and significant enhancement of storage modulus $G'(\omega)$ of the (70/30) PP/PS blend. Although analysis based on linear rheological test, i.e., SAOS test, is useful and widely used to understand the microstructure of polymer blends, it cannot fully elucidate the morphology or microstructure of polymer blends. Therefore, a nonlinear rheological test has been suggested by several researchers.

Iza et al.[27] carried out SAOS, steady shear, and transient shear tests to evaluate the effects of two different compatibilizers, styrene−ethylene/propylene−styrene (SEPS) and a random copolymer consisting of tapered hydrogenated polybutadiene−styrene, on a PS/HDPE blend. The SAOS and steady shear measurements showed no significant effect of the copolymer addition. In contrast, transient shear start-up flow demonstrated increased sensitivity to the addition of copolymers. The effects of styrene−ethylene/butylene−styrene (SEBS) copolymer on the rheological properties of a PP/PS blend were also studied by Macaubas et al.[28] Start-up measurements were conducted to evaluate nonlinear rheological properties. Elevation of stress overshoot and steady state stresses was observed upon SEBS addition to the PP/PS blend. This increase in stress overshoot was due to interfacial modifications and morphology evolutions in the SEBS-compatibilized blends. DeLeo et al.[29] found strong stress overshoots in PI-enriched PDMS/PI blends compared with PDMS-enriched blends. Specifically, the PDMS drops stuck to each other and formed droplet clusters, whereas the PI-enriched blends coalesced without sticking. These studies showed that nonlinear viscoelastic properties should be considered when seeking to induce deep changes in microstructures. Huitric et al.[30] investigated the compatibilization effects of C30B (Cloisite30B, organo-modified montmorillonite) on the rheological properties (storage modulus $G'(\omega, \gamma)$ and complex viscosity (ω)) of PE/PA-12 blends at different blend ratios and clay contents. Specifically, the SAOS test showed that the addition of C30B increased the storage modulus $G'(\omega)$ and steady shear stresses of both PE- and PA-enriched blends, which is in agreement with reduction of domain size. Moreover, it was observed that C30B was located at the interface or in PA phase due to increased affinity toward PA phase. Critical strain amplitude, defined as the limit of linearity in the strain sweep test, decreased as a function of C30B concentration.[30,31] Despite the morphological developments brought about by addition of C30B and Orevac (maleic anhydride grafted PE with M_w = 92 490 g/mol, M_n = 20 010 g/mol) as two different compatibilizers for PE/PA blends, critical strain amplitude remained constant in the case of Orevac.[31] It can be suggested that nonlinear rheological analysis should be able to detect any tiny change in morphological evolutions.

Among nonlinear rheological tests, interest in large-amplitude oscillatory shear (LAOS) test is growing. The LAOS test has been shown to be useful for the characterization of complex fluids.[32] In this test, the stress signal changes from sinusoidal to various nonsinusoidal shapes with an increase in strain amplitude, and many methods have been developed to analyze nonlinear stress signals under LAOS flow. Of these analysis methods, Fourier transform rheology (FT-rheology) was introduced to better understand and quantify the nonlinear stress responses of fluids under LAOS flow. FT-rheology decomposes the stress data in time domains into intensities in frequency domains.[33−35] These intensities are normalized by first intensities, and the third relative harmonic $[I_{3/1} \equiv I(3\omega)/I(\omega)$ where ω is the excitation angular frequency] is the most significant intensity among all higher harmonics. It has been frequently reported that FT-rheology is quite sensitive to structural changes from topological to morphological evolutions.[36−41] Vittorias et al.[39] reported that nonlinearity $(I_{3/1})$ increases upon blending of long-chain branched PE (LCB) with linear PE. The extent of this augmentation was found to be proportional to the degree of branching. Hyun and Wilhelm[42] reported in detail on changes in $I_{3/1}$ over wide ranges of strain amplitude (γ_0) and angular frequency (ω) for both linear and comb PS. They defined a nonlinear coefficient, $Q(\omega,\gamma_0) \equiv I_{3/1}/\gamma_0^2$, and the zero-strain nonlinearity, $Q_0 \equiv \lim_{\gamma_0 \to 0} Q(\omega,\gamma_0)$ where Q_0 is the asymptotic limiting and constant value of Q at low strain amplitude. It was concluded that Q_0 can distinguish between linear and comb PS. Carotenuto et al.[40] demonstrated that varying the droplet size of PDMS in a PIB matrix gives rises to different relative higher harmonics $(I_{3/1}, I_{5/1})$. In our previous work, FT-rheology was shown to sensitively capture the compatibilization effects of poly(lactic acid)/polycaprolac-

dx.doi.org/10.1021/ma500700e | Macromolecules 2014, 47, 4066−4076

tone (PLA/PCL) blends with organo-modified montmorillonite (OMMT) loading. Further, it was shown that $I_{3/1}$ increases with OMMT concentration.[41] Lim et al.[36] determined the degree of dispersion of various nanoparticles in a PCL matrix by introducing a new parameter (NLR ≡ normalized nonlinear viscoelasticity from FT-rheology/normalized linear viscoelasticity from SAOS tests). They reported that the value of NLR is quite sensitive to the dispersion quality of nanoparticles in a PCL matrix.

The majority of studies on polymer blends have focused on linear rheological properties from SAOS tests in order to investigate dispersion quality and morphology evolutions in polymer blends. In this paper, the effects of different nanoparticles (C20A and fumed silica) on (80/20) PP/PS blends were investigated in terms of their linear and nonlinear rheological properties. LAOS tests have mainly been used to examine the morphology evolution of modified blends as well as compare the compatibilization efficiencies of two types of nanoparticles. FT-rheology and another newly established parameter, NLR (nonlinear−linear viscoelastic ratio), were used to correlate rheological properties with morphological developments and interfacial tensions of the blends.

2. EXPERIMENTAL SECTION

2.1. Materials. Polypropylene (PP), HP562T ($\bar{M}_n$ = 56 000, $\bar{M}_w$ = 157 100, PDI = 2.81), used in this study was obtained from PolyMirae Company Ltd. Polystyrene (PS), HF2680 ($\bar{M}_n$ = 59 200, $\bar{M}_w$ = 168 700, PDI = 2.85), was provided by Samsung Cheil Industries Inc. Organoclay, Cloisite20A (C20A), was purchased from Southern Clay Products Inc. Cloisite20A is a dimethyl-hydrogenated tallow ammonium-modified montmorillonite with a density of 1.77 g/cm^3. Hydrophilic fumed silica (Aerosil OX 50) having a small specific surface area of 50 ± 15 m^2/g and tamped density of 0.13 g/cm^3 was purchased from Evonik Industries.

2.2. Blend Preparation. All materials were dried in a vacuum oven at 80 °C for 12 h prior to compounding. C20A and fumed silica were kept in a convection oven at 100 °C to remove excess moisture. The samples were simultaneously mixed using a Haake mixer (Thermo Fisher Scientific Inc.) at 50 rpm and 200 °C. Blend composition was 80/20 wt %, in which PP was the matrix and PS the dispersed phase. After melt blending, pellets were compressed and molded into disks with a diameter of 25 mm and thickness of 1 mm at 200 °C. In order to investigate the compatibilization effect, concentrations of 1, 3, 5, and 7 wt % were chosen for the particles (C20A and fumed silica).

2.3. Rheological Measurements. Two strain-controlled rheometers, RDA II (Rheometrics Inc.) and ARES-G2 (TA Instruments Inc.), with 25 mm parallel plate geometries were used to carry out rheological measurements. Frequency sweep tests were used to obtain linear rheological responses under small-amplitude oscillatory shear (SAOS) flow. Strain amplitudes were kept small enough (0.03−0.05) to make sure results were within linear viscoelastic regime. Nonlinear rheological properties were obtained through strain sweep tests under large-amplitude oscillatory shear (LAOS) flow with increasing strain amplitude from γ_0= 0.01 to 5 at a fixed frequency of 1 rad/s. All measurements were carried out at 180 °C.

2.4. Morphology. Field emission scanning electron microscopy (FE-SEM) observations were carried out using a JSM 6700F microscope at 5 kV to evaluate morphology evolutions. Samples were fractured in liquid nitrogen and then covered with platinum. The number-average radius (R_n) and volume average radius (R_v) were calculated using eqs 1 and 2. Radii of over 150 droplets were calculated using image analyzer software (ImageJ).

$$R_n = \frac{\sum n_i R_i}{\sum n_i} \quad (1)$$

$$R_v = \frac{\sum n_i R_i^4}{\sum n_i R_i^3} \quad (2)$$

In eqs 1 and 2, n_i is the number of droplets with radius R_i. Locations of C20A and fumed silica were observed by transmission electron microscopy (TEM) using a FEI Tecnai G^2 T-20s at an accelerating voltage of 200 kV. Samples were cut using a cryo-microtome device at −140 °C and put on a copper grid.

3. RESULTS AND DISCUSSION

3.1. Dynamic Oscillatory Shear Tests. Small-amplitude oscillatory shear (SAOS) tests were carried out at 180 °C at a fixed strain amplitude of γ_0 = 0.03−0.05 within the linear regime. Absolute values of complex moduli $|G^*(\omega)|$ of the virgin polymers PP and PS as well as the uncompatibilized blend of (80/20) PP/PS are shown in Figure 1. According to

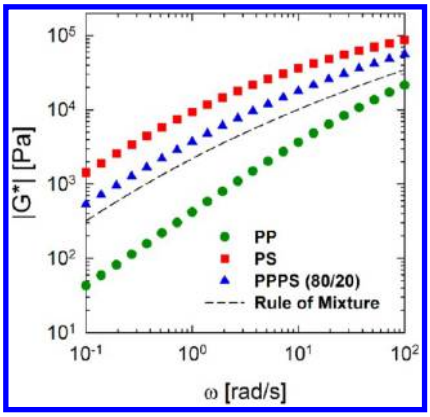

Figure 1. Complex moduli $|G^*(\omega)|$ of the virgin polymers PP and PS as well as the uncompatibilized (80/20) PP/PS blend as a function of frequency at 180 °C and a fixed strain amplitude of 0.05.

the results, the $|G^*(\omega)|$ of the (80/20) PP/PS blend was somewhat between the neat components and close to the log additivity mixing rule, $\log|G^*(\omega)|_{mix} = \sum w_i \log|G^*(\omega)|_i$ where w_i is the weight fraction and $|G^*(\omega)|_i$ is the complex moduli magnitude of the components. The storage and loss moduli showed the same behavior (not shown here).

Figure 2a and 2b demonstrate the effects of C20A and fumed silica concentrations on linear rheological properties, $|G^*(\omega)|$, respectively. Elevation of clay weight fractions increased the moduli of the blends. These results are consistent with previous studies in which clay loadings increased moduli of the immiscible blends.[4,16,41] This enhancement of the moduli could be due to either reinforcing effect related to inter- and intraparticle interactions or compatibilizing effects when located at interface.[14,36,43] However, this improved modulus of the (80/20) PP/PS blend was less evident in the case of hydrophilic fumed silica-incorporated blends (Figure 2b).

Nanoparticles selectively located in one of the phases and changed the viscosity ratios or acted as interfacial agents when accommodated at the interface (will be discussed later). Although addition of particles relatively enhanced the linear viscoelastic behaviors of the blends (see inside of Figure 2), it is worth noting that the viscoelastic responses of the polymers in practical situations are no longer linear, resulting in either breakup or coalescence of the drops. A broad distribution of droplet sizes, especially in the case of uncompatibilized blend, indicates coexistence of breakup and coalescence,[44] whereas small and large droplets can be seen in Figure 4 as a result of

dx.doi.org/10.1021/ma500700e | Macromolecules 2014, 47, 4066−4076

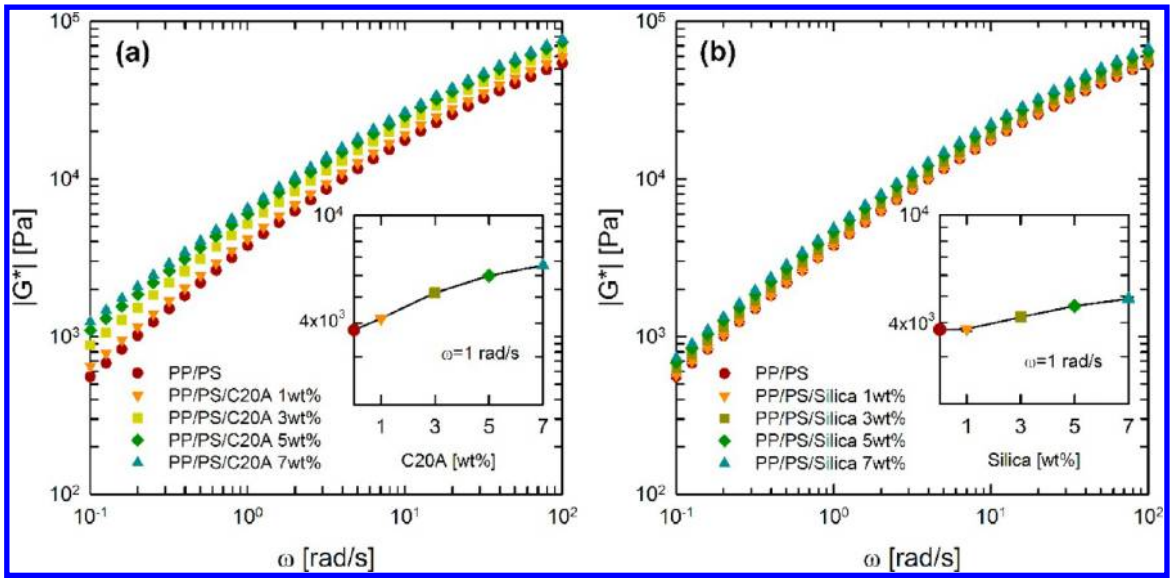

Figure 2. Absolute magnitude of complex modulus $|G^*(\omega)|$ as a function of frequency at various (a) clay concentrations and (b) fumed silica concentrations of (80/20) PP/PS blends at 180 °C and a fixed strain amplitude of 0.03. Inside figures in both (a) and (b) show complex modulus $|G^*|$ as a function of concentration at a fixed frequency of ω = 1 rad/s.

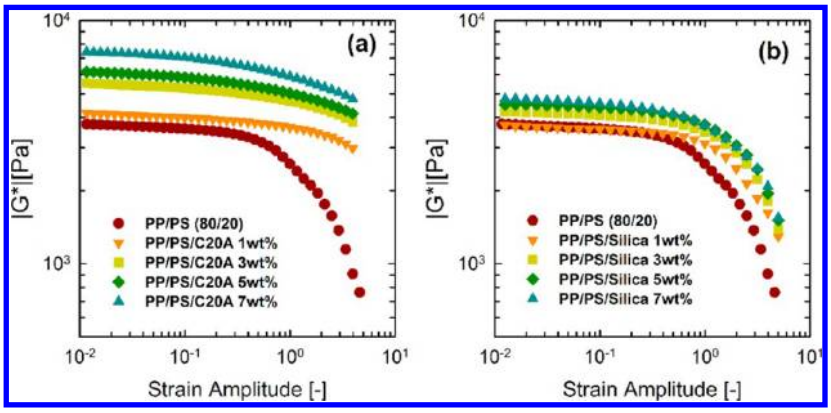

Figure 3. Absolute magnitude of complex modulus $|G^*(\gamma_0)|$ as a function of strain amplitude for various concentrations of (a) PP/PS/C20A and (b) PP/PS/silica blends at 180 °C and a fixed frequency of 1 rad/s.

breakup and coalescence, respectively. However, this was eliminated to some extent when particles, more specifically C20A, were added to the blends. Therefore, LAOS tests were conducted to probe the nonlinear responses of the blends. Figure 3a and 3b show the complex moduli $|G^*(\gamma_0)|$ of the PP/PS/C20A and PP/PS/silica blends at a fixed frequency of 1 rad/s under LAOS flow. Similar to the SAOS results, silica particles were less effective in improving rheological properties, as growth of the complex modulus of the 7 wt % silica-loaded blend was less than that of the 3 wt % C20A-loaded blend. In contrast, when silica particles were loaded, no remarkable changes were observed in either linear range properties or magnitude of the moduli. Therefore, silica particles could be mostly aggregated inside the PS phase, and the slight increase in moduli could be due to reinforcing effects of silica particles (discussed later). Since there is interplay between rheological and morphological properties, study of morphological properties of the corresponding blends is of great interest.

To observe how different types of particles affect morphological evolutions of the blends, SEM images of the two blend systems were compared (Figure 4). The results show that incorporation of C20A particles led to a remarkable decrease in PS droplet size up to an optimum level (5 wt %), after which any further increase in C20A concentration had no significant effect on droplet size. On the other hand, droplet size remained unchanged upon addition of silica particles. This can be attributed to decreased particle−polymer interactions due to the very low surface area per unit volume of this particular silica (OX50). Figure 5 compares the number-average radii R_n and volume average radii R_v of PP/PS/silica blend with those of PP/PS/C20A blend as a function of concentration. It is suggested that the nature of the particles plays a crucial role in determining morphological evolutions.

Of note, localization of particles could also be a determining factor when dealing with morphological evolutions of the particle-induced blends.[16,45] Notably, organoclays located at the interface can facilitate compatibilization effects in immiscible polymer blends.[16] Therefore, TEM was used to determine the locations of the fillers. As shown in Figure 6, C20A particles were located at the interface (more thermodynamically stable phase) at lower concentrations. Thickness of the interface layer, where clays build up a layer around PS phase, increased from 6 nm at 1 wt % to 30 nm at 5 wt %. As clay content increased, some extra amounts of C20A became located inside PS phase

dx.doi.org/10.1021/ma500700e | Macromolecules 2014, 47, 4066−4076

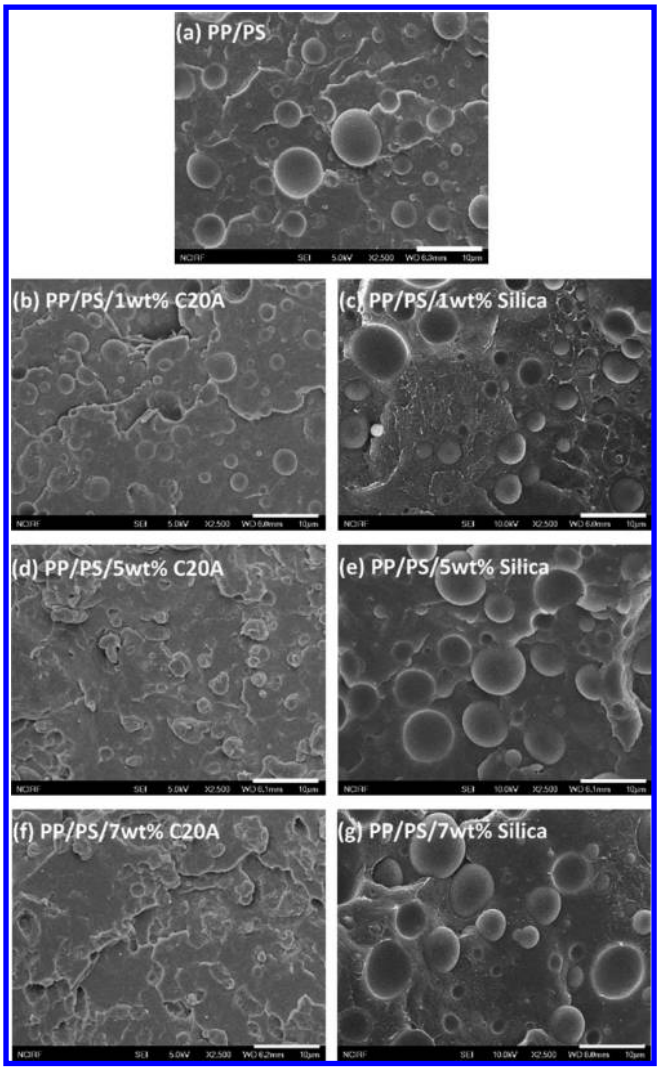

Figure 4. SEM images of the (a) PP/PS, (b) PP/PS/1 wt % C20A, (c) PP/PS/1 wt % silica, (d) PP/PS/5 wt % C20A, (e) PP/PS/5 wt % silica, (f) PP/PS/7 wt % C20A, and (g) PP/PS/7 wt % silica blends. Scale bar is 10 μm for all figures.

(more compatible phase) (Figure 6g,h). As deformation of the minor phase was exacerbated due to the increased viscosity of PS dispersed phase, size reduction at high concentrations was hindered. In contrast, TEM images of PP/PS/silica blends revealed a cluster of silica particles mainly inside PS phase and not at the interface (Figure 7a,b). In fact, less particle−polymer interactions and highly agglomerated particles impeded enhancement of compatibility between PP and PS phase (Figure 7b). It is worth remembering that the moduli of the filler-induced systems have three contributions—hydrodynamic effect due to the filler geometry, viscoelastic effect, and an interparticle network[43]—as droplet size remained constant, and agglomerated silica particles formed inside the PS phase. Therefore, increases in the complex moduli of the PP/PS/silica blends can be attributed to the hydrodynamic effects of the silica particles, which are caused by a higher number of silica particles per unit volume.[43]

Moreover, these findings suggest that particle orientation in a blend system is an important factor to consider when investigating morphological evolutions. With increasing C20A content, the interface of dispersed phase was covered with sufficient particles and droplets were stabilized. When particles located at the interface, drainage of the matrix film between two closing droplets becomes hindered as a result of an interfacial tension gradient caused by Marangoni stresses. This mechanism as well as steric repulsion between the clays enveloping the PS droplets suppress coalescence, leading to smaller droplet sizes.[3,16,44] Furthermore, this decline in droplet size upon C20A addition could be due to reduction of interfacial tension caused by breakup of the droplets.[23,28] Thus, information on interfacial tensions could provide approximate insights into morphological evolutions.

3.2. Interfacial Tension Analysis. The Gramespacher and Meissner model[20] was used to evaluate interfacial tensions from rheological measurements using weighted relaxation spectra. Based on their model, the shear modulus of a blend is considered as a combination of each phase's (matrix and dispersed phases) contributions as well as the interfacial contribution. As a result of their research, three peaks were observed in the relaxation spectrum of a blend. Two of them were shown to be associated with the relaxation times of each

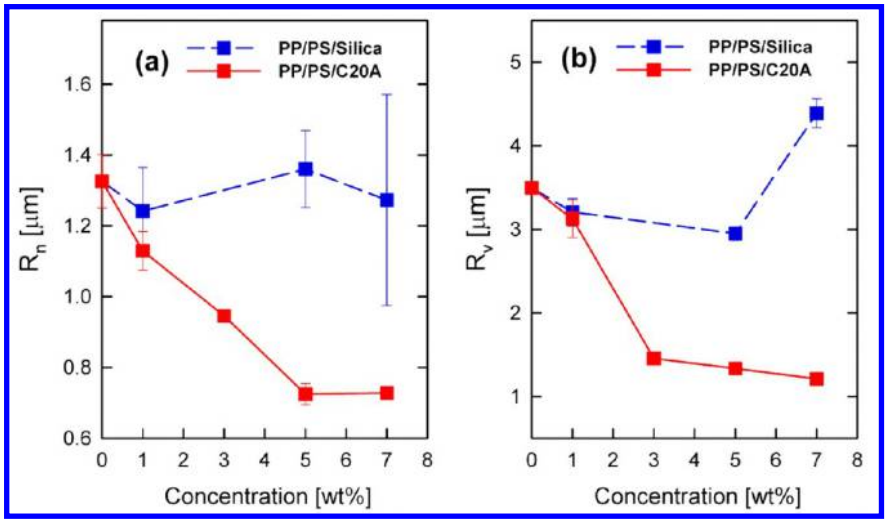

Figure 5. (a) Number-average radius R_n and (b) volume-average radius R_v of the PP/PS, PP/PS/C20A, and PP/PS/silica blends as a function of nanoparticle concentration. A minimum of 150 droplets was selected to calculate the radii size distributions for each composition.

dx.doi.org/10.1021/ma500700e | Macromolecules 2014, 47, 4066−4076

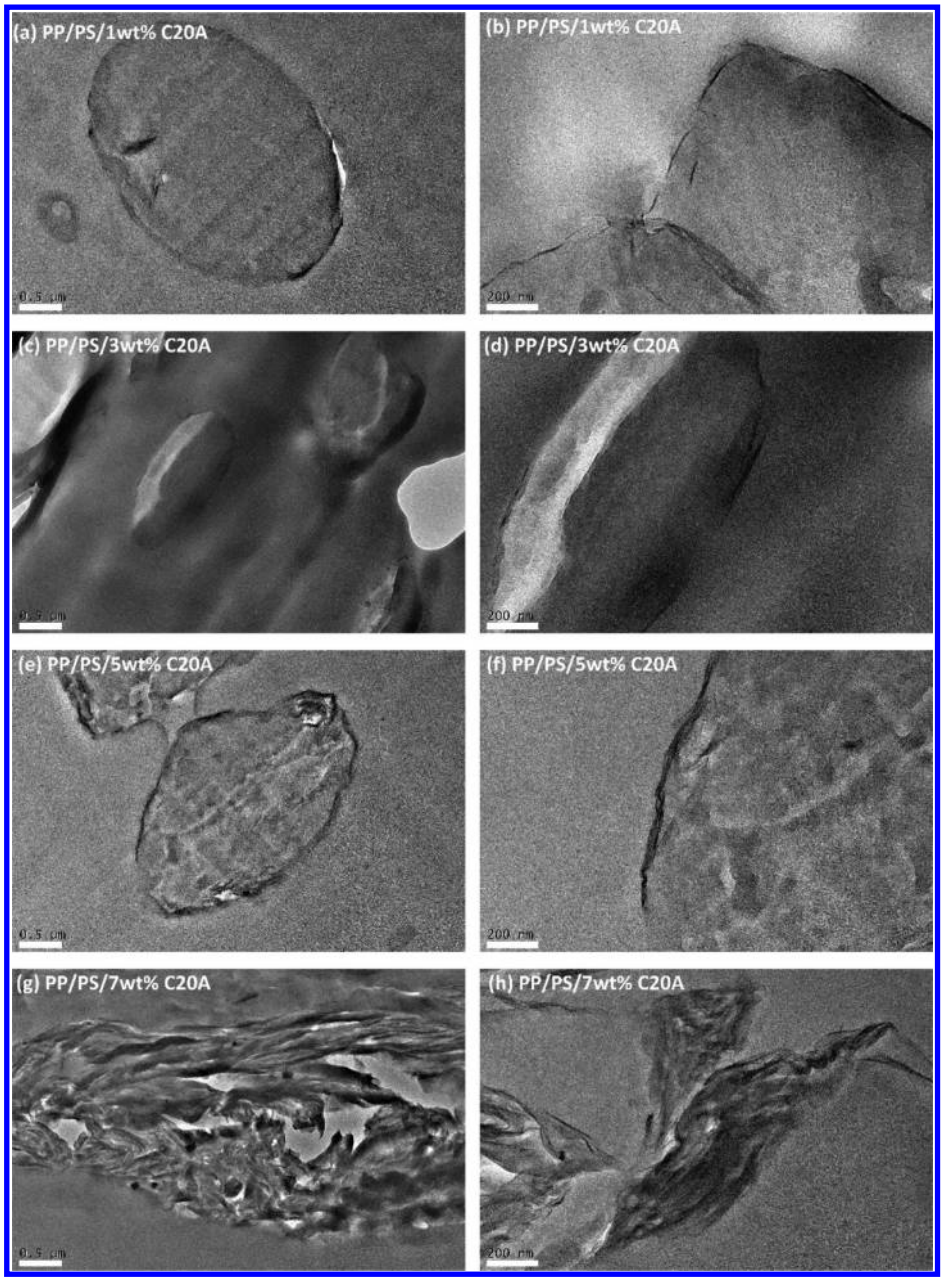

Figure 6. TEM images of (a, b) PP/PS/1 wt % C20A, (c, d) PP/PS/3 wt % C20A, (e, f) PP/PS/5 wt % C20A, and (g, h) PP/PS/7 wt % C20A. Scale bar is 0.5 μm for the left-hand side figures and 200 nm for the right-hand side figures.

phase, whereas the remaining longest one was shown to be related to the form relaxation time (τ_1) of the dispersed droplets. Form relaxation time is the characteristic time associated with the retraction process of deformed droplets to their original spherical shape.[24] Thus, interfacial tension between phases of the blend can be inferred from this third peak using the equation

$$\alpha = \left[\frac{R_v \eta_m}{\tau}\right]\left[\frac{(19K+16)(2K+3)}{40(K+1)}\right]\left[1+\phi\left(\frac{5(19K+16)}{4(K+1)(2K+3)}\right)\right] \quad (3)$$

where R_v is the volume average domain radius, η_m is the zero-shear viscosity of the matrix phase, ϕ is the volume fraction of the dispersed phase, τ is the form relaxation time, K is viscosity ratio η_d/η_m, and η_d is the zero-shear viscosity of the dispersed phase. Note that the model presented by Gramespacher and Meissner[20] was basically derived for dilute systems, which means that the coalescence effect was neglected in preliminary assumptions. Since the polymer blend is not a dilute system, the volume average droplet size (R_v) in eq 3 contains coalescence effect. Moreover, in concentrated blend systems, there is a wide distribution of particle size. Because of these two reasons, quantitative analysis of interfacial tension is a somewhat questionable task. However, qualitative study of interfacial tension could be performed to provide an estimation of interfacial tension trends.[20] Considering these assumptions and using eqs 2 and 3 and the values given in Table 1, interfacial tensions of compatibilized and uncompatibilized blends were estimated. The values of the estimated interfacial tensions and relaxation times of the blends are shown in Table 2. The fixed-point iteration method, proposed by Cho and Park,[46] was used to calculate the weighted relaxation spectra in

dx.doi.org/10.1021/ma500700e | Macromolecules 2014, 47, 4066−4076

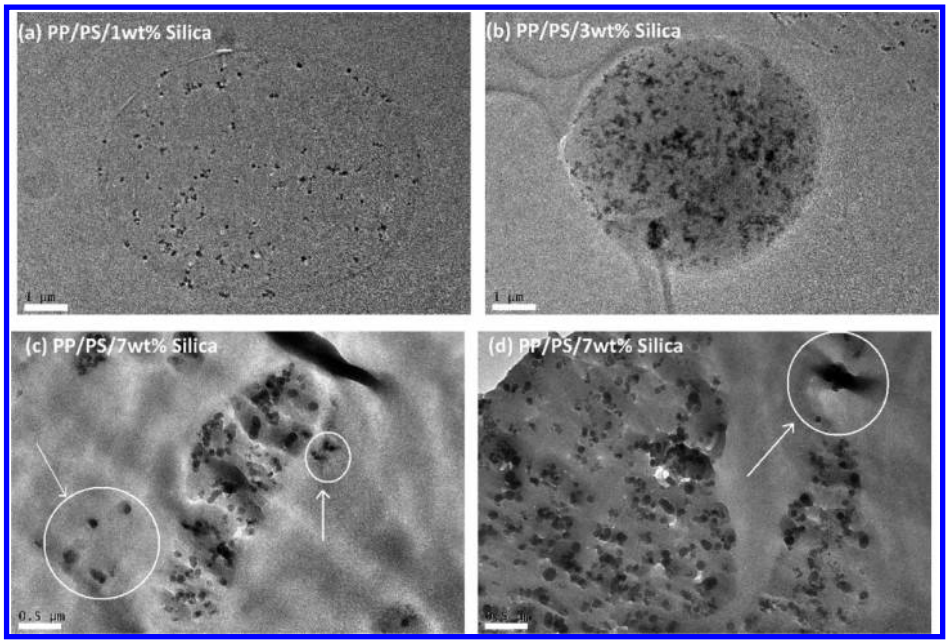

Figure 7. TEM images of the (a) PP/PS/1 wt % silica, (b) PP/PS/3 wt % silica, and (c, d) PP/PS/7 wt % silica. Scale bar is 1 μm for (a, b) and 0.5 μm for (c, d).

Table 1. Parameters Required for Interfacial Calculations at 180 °C

parameter	values
zero-shear viscosity of the matrix PP (η_m)	4.25×10^2 Pa s
zero-shear viscosity of the dispersed phase PS (η_d)	1.66×10^4 Pa s
viscosity ratio $K = \eta_d/\eta_m$	39
volume fraction of the dispersed phase PS ϕ	0.17 ± 0.005

Table 2. Calculated Interfacial Tensions and Form Relaxation Time Values of the Blends Incorporated with C20A and Fumed Silica[a]

filler content [%]	α_{C20A} [mN/m]	α_{silica} [mN/m]	τ_{C20A} [s]	τ_{silica} [s]	$R_{v_{C20A}}$ [μm]	$R_{v_{silica}}$ [μm]
0	1.9	1.9	31.62	31.62	3.5	3.5
1	1.69	1.3	31.62	42.16	3.12	3.2
3	0.59		42.16	42.16	1.45	
5	0.4	1.59	56.23	31.62	1.33	2.94
7	0.36	3.16	56.23	23.71	1.21	4.39

[a]The fixed-point iteration method was used to calculate the weighted relaxation spectra.[46]

this study. Weighted relaxation of the each component is shown in Figure 8a,b.

The weighted relaxation spectra of the neat components reveal that the peak associated with pure PP was too small and detected ($\tau \approx 8.0 \times 10^{-3}$ s) within a very short time when overlapped with PS, which showed a peak at around $\tau \approx 1.77$ s (see Figure 8). Alternatively, the weighted relaxation spectra of the PP/PS/C20A and PP/PS/silica blends are plotted in Figures 9a,9b, respectively. These weighted relaxation spectra are calculated from SAOS test. To obtain high relaxation time region, SAOS tests were carried out from $\omega = 0.01$ to 100 rad/s (usually from $\omega = 0.1$ to 100 rad/s; see Figure 2).

Since the peak associated with neat PP was too small to be clearly seen in the overlapped curves of the blends and the peak appearing around $\tau \approx 1.77$ s is accounted for the dispersed phase of PS, it can be assumed that the remaining peak at longer times is related to the form relaxation time of the dispersed droplets. Figure 9a demonstrates that the weighted relaxation spectra sharply increases at longest relaxation times due to the corresponding larger dynamic moduli of the compatibilized blends at lower frequencies.[20] This result becomes even more interesting when comparing Figures 9a and 9b. Relaxation spectra of the PP/PS/silica blends were much lower than those of the PP/PS/C20A blends, indicating their slightly higher efficiencies in enhancing rheological properties. A broad peak in the PP/PS/C20A blends is due to the broad distribution of droplet size. Figure 9a,b and the values presented in Table 2 show that relaxation time related to the form relaxation process of the dispersed phase shifted to higher values when C20A and fumed silica were added to the blend up to a certain concentration (5 wt % for C20A and 1 wt % for fumed silica). To put this result in context, relaxation of the interface can be attributed to a balance between two forces: a shearing force, proportional to $\eta\dot{\gamma}$ (where η is the viscosity and $\dot{\gamma}$ is the shear rate), that tends to deform the dispersed phase droplets and a cohesive force, proportional to the ratio α/d (where α is the interfacial tension between two polymers and d is the diameter of the droplet), that contributes to retraction of the dispersed phase into a spherical shape. This proportional relationship between relaxation time values and C20A concentration indicates that the shearing force is larger than the cohesive force.[20,23]

On the other hand, the longest relaxation time of PP/PS/silica blends shifted to lower times at high silica contents. That is reason why some of the silica particles are located outside of the PS phase. It is shown in Figure 7c,d.

Sundarraraj and Macosko[44] reported that the main contribution of droplet-sized compatibilizers is the suppression of coalescence rather than interfacial tension reduction, which is neglected in Gramespacher and Meissner's model. Thus, the values of interfacial tensions reported in Table 2 are not exact values, but they can be used as a qualitative approximation of interfacial tensions.

dx.doi.org/10.1021/ma500700e | Macromolecules 2014, 47, 4066−4076

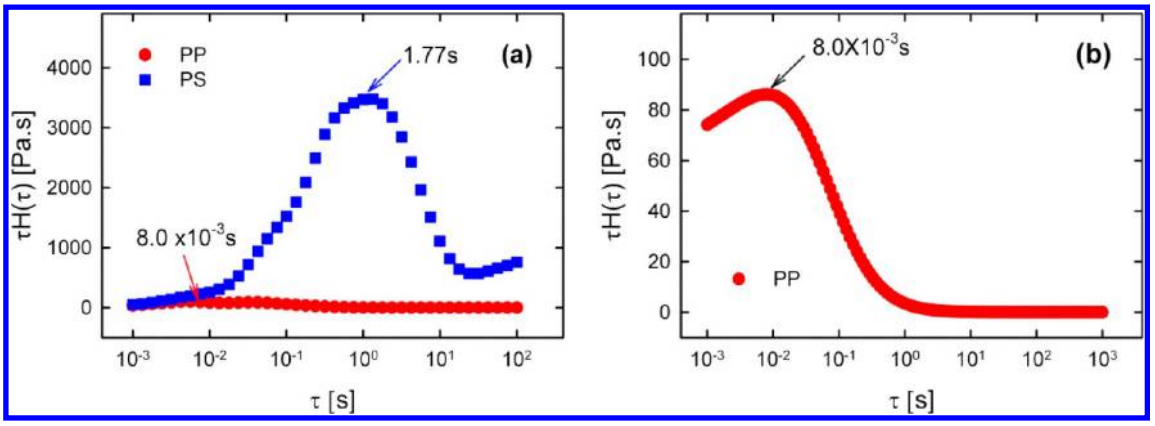

Figure 8. (a) Weighted relaxation spectra of neat PP and PS at 180 °C. The peaks associated with PP and appear at 1.77 and 8.0 × 10^{-3} s, respectively. (b) Zoomed-in, higher resolution weighted relaxation spectra of PP at 180 °C.

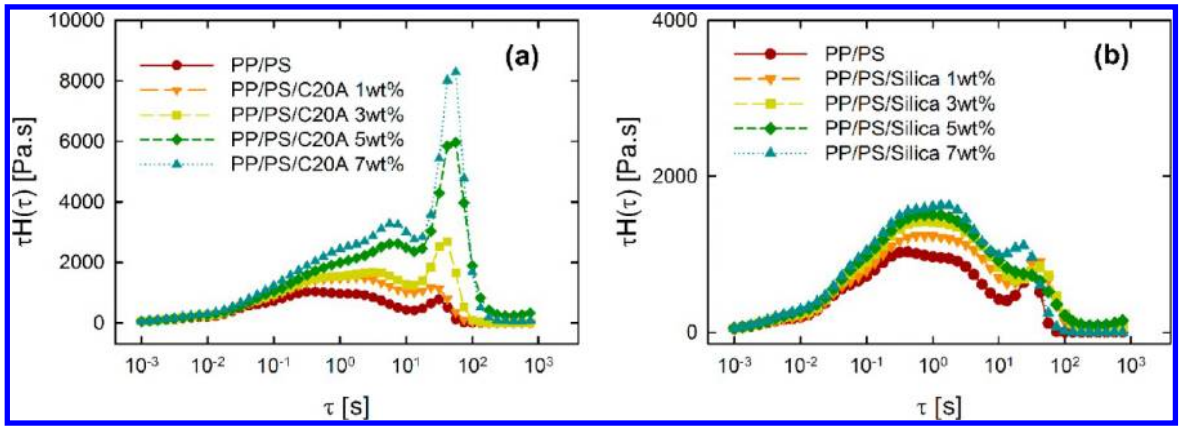

Figure 9. Weighted relaxation spectra of (a) PP/PS/C20A and (b) PP/PS/silica blends at various C20A and fumed silica concentrations (wt %) at 180 °C.

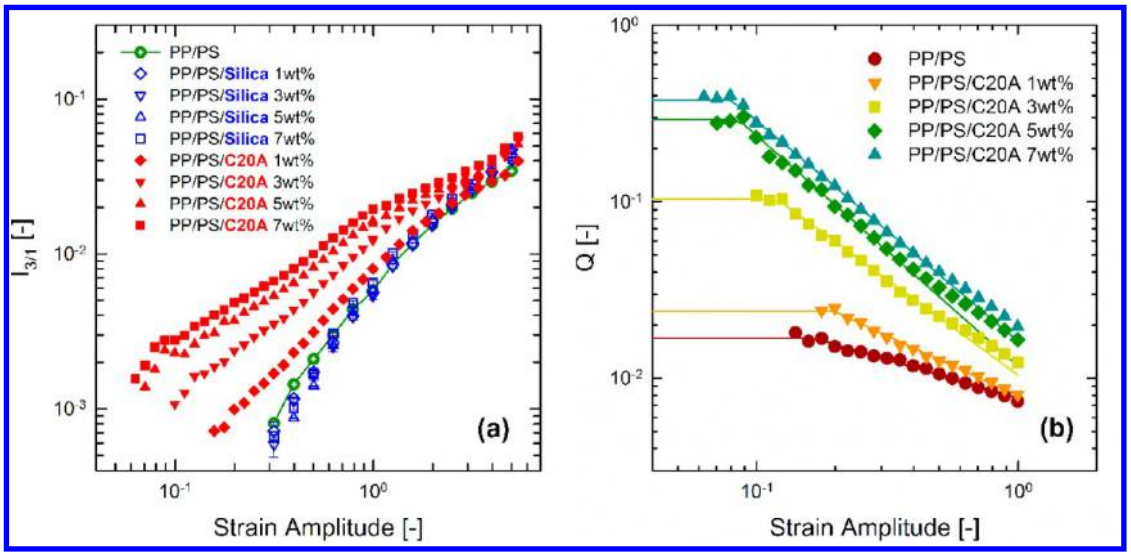

Figure 10. (a) Normalized third relative intensities ($I_{3/1}$) as a function of strain amplitude for PP/PS, PP/PS/C20A (filled red color symbol), and PP/PS/silica (unfilled blue color symbol) blends. (b) Q parameters of the PP/PS and PP/PS/C20A blends at 180 °C and a fixed frequency of 1 rad/s. Solid lines are the fitted results from the mathematical model.

3.3. Fourier Transform Rheology (FT-Rheology). FT-rheology was applied to quantify the nonlinear response in order to better understand internal structures. Grosso and Maffettone[47] established a model based on LAOS flow that could estimate the droplet size distributions of immiscible polymer blends using FT-rheology. Reinheimer et al.[48] proposed another theoretical model in which nonlinear features (odd relative intensities) are correlated with interfacial tension as well as the droplet size of a dilute emulsion. They concluded that interfacial tension or droplet size could be estimated if

dx.doi.org/10.1021/ma500700e | Macromolecules 2014, 47, 4066−4076

either parameter is known. The normalized third relative intensities $I_{3/1}$ of the PP/PS/C20A and PP/PS/silica blends as a function of strain amplitude are plotted in Figure 10a. Reinheimer et al.[48] reported that nonlinearity ($I_{3/1}$) is related to the inverse of interfacial tension based on a theoretical model for emulsion systems. Qualitative analysis from Gramespacher and Meissner's model revealed that interfacial tension of the PP/PS/C20A blends decreased with increasing concentration of C20A (see Table 2). Therefore, nonlinearity ($I_{3/1}$) of the PP/PS/C20A blend should increase with increasing concentration of C20A. This result is consistent with the experimental results in Figure 10a. However, in the case of the PP/PS/silica blend, nonlinearity ($I_{3/1}$) did not change much compared with that of the PP/PS/C20A blend, which is consistent with the SEM and TEM images showing that silica did not improve the interface of the PP/PS blends. Hyun and Wilhelm[42] defined a nonlinear coefficient, $Q(\omega,\gamma_0) \equiv I_{3/1}/\gamma_0^2$ from FT-rheology. $Q_0(\omega) \equiv \lim_{\gamma_0 \to 0} Q(\omega,\gamma_0)$ was proposed as the asymptotic value for the Q parameter at small strain amplitude, named the zero-strain nonlinear coefficient. The nonlinear parameter Q is fitted using a mathematical model $[Q = Q_0(1 + (C_1\gamma_0)^{C_2})^{(C_3-1)/C_2}]$ similar to the Carreau–Yasuda viscosity equation.[36] Zero-strain nonlinear coefficient (Q_0), critical strain amplitude ($\gamma_{0c} = 1/C_1$), and the degree of strain thinning (C_3) can be estimated using the fitting results. Q parameters as a function of strain amplitudes for the PP/PS/C20A blends as well as the fitting results are plotted in Figure 10b. Q parameters of the PP/PS/silica blends are not shown here for the sake of clarity. The fitting results are shown in Tables 3 and 4 for the PP/PS/C20A and PP/PS/silica blends, respectively.

Table 3. Fitting Results of the PP/PS/C20A Blends at Different Clay Concentrations

composition	Q_0	$C_1 = 1/\gamma_{0c}$	C_2	C_3
PP/PS	0.0169	6.06	22.48	0.5650
PP/PS/1 wt % C20A	0.0240	5.05	439.38	0.3148
PP/PS/3 wt % C20A	0.1038	8.37	333.80	−0.0813
PP/PS/5 wt % C20A	0.2936	11.79	288.14	−0.3064
PP/PS/7 wt % C20A	0.3752	12.37	282.57	−0.2483

The nonlinear parameter Q increased when C20A concentration increased, which indicates that the morphologies of the blends changed. Fitted results revealed that Q_0 and critical strain amplitude remained unchanged when silica particles were added, indicating that silica particles did not improve nonlinear rheological properties. These results are consistent with the SEM images, in which drop sizes did not change as silica concentrations increased. In contrast, C20A particles reduced critical strain amplitude as their concentration increased. These results are also consistent with the SEM images, in which drop sizes decreased with increasing C20A concentration.

Recently, Lim et al.[36] proposed a new parameter, nonlinear–linear viscoelastic ratio (NLR), defined as follows:

$$\mathrm{NLR} = \frac{Q_0(\phi)/Q_0(0)}{|G^*(\phi)|/|G^*(0)|} \quad (4)$$

where ϕ is the filler concentration. In the case of NLR = 1, the effect of nonlinear viscoelasticity is the same as the effect of linear viscoelasticity as the concentration increases. In the case of NLR > 1, the nonlinear parameter is amplified more than the linear parameter due to internal structure. In the case of NLR < 1, the nonlinear parameter is amplified less than the linear parameter. Lim et al.[36] found that NLR as a new established parameter can amplify microstructural changes more precisely than only using linear rheological properties such as complex modulus $|G^*(\omega)|$ or nonlinear rheological properties such as Q_0. As shown in Figure 2, the complex moduli $|G^*(\omega)|$ of both the PP/PS/C20A and PP/PS/silica blends increased with increasing filler concentration. Linear rheological properties mainly reflect three contributions: polymer, interfacial tension, and filler (or particle). Thus, complex modulus $|G^*(\omega)|$ is strongly affected by the existence of filler (inorganic solid) itself. Addition of particles could increase linear rheological properties. Therefore, NLR was used to investigate changes in morphology according to the particles used in this study. NLR values of the PP/PS/C20A and PP/PS/silica blends were calculated and compared in order to correlate the rheological response to morphology changes in this particular blend system. As shown in Figure 11, NLR values were larger than 1

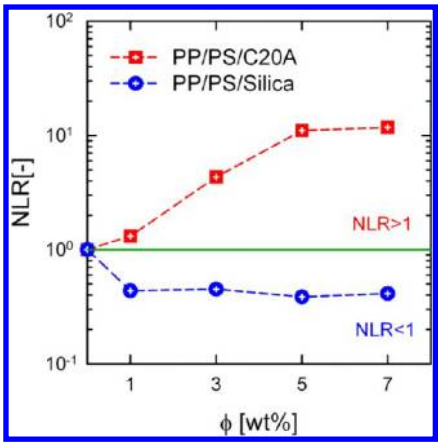

Figure 11. Comparison of NLR values of PP/PS/C20A and PP/PS/silica blends as a function of weight fraction of particles.

(NLR > 1) for the PP/PS/C20A blends, and they increased only up to a certain clay content (5 wt %) at which point further incorporation of clays did not have significant effects on morphologies. For example, the highly concentrated blend (7 wt %) showed aggregation of clay into stacks. On the other hand, NLR values of the PP/PS/silica blends were constantly below 1 (NLR < 1). These two NLR values are due to

Table 4. Fitting Results of PP/PS/Silica Blends in Three Experiments for Each Composition

composition	Q_0	$C_1 = 1/\gamma_{0c}$	C_2	C_3
PP/PS/1 wt % silica	0.00717 ± 0.00017	0.8995 ± 0.0367	2.713 ± 0.301	0.02928 ± 0.03025
PP/PS/3 wt % silica	0.00817 ± 0.00061	0.9778 ± 0.1947	4.101 ± 0.208	0.05887 ± 0.09134
PP/PS/5 wt % silica	0.00771 ± 0.00065	0.7903 ± 0.0064	5.532 ± 1.499	−0.02537 ± 0.04219
PP/PS/7 wt % silica	0.00877 ± 0.00063	0.8671 ± 0.14579	4.601 ± 1.058	−0.0464 ± 0.10976

dx.doi.org/10.1021/ma500700e | Macromolecules 2014, 47, 4066–4076

interfacial tension differences. As two different particles were added, linear rheological property $|G^*(\omega)|$ increased with increasing particle concentrations (see inside of Figure 2). However, nonlinear rheological property Q_0 only increased when interfacial tension decreased, i.e., only in the case of C20A. Thus, nonlinear−linear viscoelastic ratio (NLR) could be categorized into NLR > 1 or NLR < 1. Interestingly, NLR values were found to be inversely proportional to droplet size changes in PP/PS/C20A. Further, NLR values of PP/PS/C20A blends reached a plateau from 5 wt %. The NLR value of 7 wt % C20A was found to be the same as that of C20A 5 wt %. This result is consistent with the droplet size results in Figures 4 and 5. Therefore, additional C20A cannot improve the morphologies of PP/PS blends anymore. In the case of PP/PS/silica blends, NLR values showed the same values even though the silica concentration increased, which is consistent with the droplet size results in Figures 4 and 5. Therefore, silica could not improve morphology, whereas NLR maintained a constant value as a function of silica concentration. Based on these results, NLR value could actually detect evolutions of morphologies, whereas moduli of the blends only increased due to volumetric effects of the fillers.[43]

The NLR value as determined by dynamic oscillatory shear test (both SAOS and LAOS) can be a promising tool to estimate internal structural changes in polymer blends in a relatively more straightforward and cost-effective manner compared to interfacial tension calculations and microscopic analysis. It is important to note that NLR value reflects rheological and morphological contributions, including moduli, interfacial tensions, and droplet size information, and application of this empirical parameter is not limited to the type of multiphase system (dilute suspensions, polymer melt blends, or composites). Moreover, both rheological and optical results revealed that C20A clays can act as compatibilizers for this particular (80/20) PP/PS blend, whereas fumed silica particles did not exhibit such characteristics.

4. CONCLUSION

Compatibilization effects of two different nanoparticles (C20A and fumed silica) on the same blend system PP/PS (80/20) at different particle concentrations were investigated. Both SAOS (small-amplitude oscillatory shear) and LAOS (large-amplitude oscillatory shear) tests revealed increased efficiencies of the C20A clays in enhancing rheological properties compared to silica, and the tests confirmed the compatibilization effects of C20A clays for this (80/20) PP/PS blend. Interfacial tension calculations based on Gramespacher and Meissner's model showed that C20A particles reduced the interfacial tensions of (80/20) PP/PS blends while hydrophilic fumed silica particles were unable to improve interfacial and morphological properties. The new NLR parameter was used to compare the effects of particles on morphologies of the blends. The NLR parameter was found to be inversely proportional to droplet size changes as well as able to detect the optimum morphological status. NLR values of the PP/PS/C20A blends gradually increased up to an optimum weight fraction (5 wt %) and reached a plateau region afterward (NLR > 1). In contrast, NLR values of the PP/PS/silica blends followed a plateau line below 1 and were much lower than those of the PP/PS/C20A blends (NLR < 1). These results are consistent with the SEM and TEM images. From the TEM images, clay was located mostly at the interface or partially inside the PS drops. Therefore, clay increased the dispersion morphologies of the PP/PS blends. In contrast, fumed silica was located mostly inside the PS droplets, which means the morphologies of PP/PS blends were not improved. These differential effects of the particles on blend morphology demonstrate two categories for NLR values, i.e., NLR larger than one (NLR > 1) and NLR less than one (NLR < 1). These findings further reveal that the NLR parameter is quite sensitive to small changes in the internal structures of the polymer blends. Furthermore, application of this empirical parameter is not limited to the type of multiphase system (dilute suspensions, polymer melt blends, or composites).

AUTHOR INFORMATION

Corresponding Author

*E-mail kyuhyun@pusan.ac.kr (K.H.).

Notes

The authors declare no competing financial interest.

ACKNOWLEDGMENTS

This research was supported by the Basic Science Research Program through the National Research Foundation of Korea (NRF) (No. 2010-0024466) and BK21 PLUS Centre for Advanced Chemical Technology (21A20131800002).

REFERENCES

(1) Fayt, R.; Jerome, R.; Teyssie, P. *J. Polym. Sci., Polym. Lett. Ed.* **1981**, 79−84.
(2) Gleinser, W.; Braun, H.; Friedricht, C.; Cantow, H. J. *Polymer* **1994**, *35*, 128−135.
(3) Van Puyvelde, P.; Velankar, S.; Moldenaers, P. *Curr. Opin. Colloid Interface Sci.* **2001**, *6* (5), 457−463.
(4) Ray, S. S.; Pouliot, S.; Bousmina, M.; Utracki, L. A. *Polymer* **2004**, *45* (25), 8403−8413.
(5) Utracki, L. A.; Sammut, P. *Polym. Eng. Sci.* **1988**, *28* (21), 1405−1415.
(6) Utracki, L. A. *J. Rheol.* **1991**, *35*, 1615−1637.
(7) Brahimi, B.; Ait-Kadi, A.; Ajji, A.; Jerome, R.; Fayt, R. *J. Rheol.* **1991**, *35*, 1069−1091.
(8) Van Hemelrijck, E.; Van Puyvelde, P.; Velankar, S.; Macosko, C. W.; Moldenaers, P. *J. Rheol.* **2003**, *48*, 143−158.
(9) Van Hemelrijck, E.; Van Puyvelde, P.; Moldenaers, P. *Macromol. Symp.* **2006**, *233* (1), 51−58.
(10) Ismail, H.; Nasir, M. *Polym. Test.* **2002**, *21* (2), 163−170.
(11) Asthana, H.; Jayaraman, K. *Macromolecules* **1999**, *32* (10), 3412−3419.
(12) Raghu, P.; Nere, C. K.; Jagtap, R. N. *J. Appl. Polym. Sci.* **2003**, *88* (2), 266−277.
(13) Slouf, M.; Radonjic, G.; Hlavata, D.; Sikora, A. *J. Appl. Polym. Sci.* **2006**, *101* (4), 2236−2249.
(14) Cassagnau, P. *Polymer* **2008**, *49* (9), 2183−2196.
(15) Wang, Y.; Zhang, Q.; Fu, Q. *Macromol. Rapid Commun.* **2003**, *24* (3), 231−235.
(16) Hong, J. S.; Kim, Y. K.; Ahn, K. H.; Lee, S. J.; Kim, C. *Rheol. Acta* **2007**, *46* (4), 469−478.
(17) Hong, J. S.; Kim, Y. K.; Ahn, K. H.; Lee, S. J. *J. Appl. Polym. Sci.* **2008**, *108* (1), 565−575.
(18) Palierne, J. F. *Rheol. Acta* **1990**, *29*, 204−214.
(19) Choi, S. j.; Schowalter, W. R. *Phys. Fluids* **1975**, *18*, 420−427.
(20) Gramespacher, H.; Meissner, J. *J. Rheol.* **1992**, *36*, 1127−1141.
(21) Jacobs, U.; Fahrländer, M.; Winterhalter, J.; Friedrich, C. *J. Rheol.* **1999**, *43*, 1495−1509.
(22) Sung, Y. T.; Han, M. S.; Hyun, J. C.; Kim, W. N.; Lee, H. S. *Polymer* **2003**, *44* (5), 1681−1687.
(23) Souza, A. M. C.; Demarquette, N. R. *Polymer* **2002**, *43* (14), 3959−3967.
(24) Riemann, R. E.; Cantow, H. J.; Friedrich, C. *Macromolecules* **1997**, *30* (18), 5476−5484.

(25) Li, Y. Y.; Hu, S. W.; Sheng, J. *Eur. Polym. J.* **2007**, *43* (2), 561−572.
(26) Cho, S.; Hong, J. S.; Lee, S. J.; Ahn, K. H.; Covas, J. A.; Maia, J. M. *Macromol. Mater. Eng.* **2011**, *296* (3−4), 341−348.
(27) Iza, M.; Bousmina, M.; Jérôme, R. *Rheol. Acta* **2001**, *40* (1), 10−22.
(28) Macaúbas, P. H.; Demarquette, N. R.; Dealy, J. M. *Rheol. Acta* **2005**, *44* (3), 295−312.
(29) DeLeo, C.; Walsh, K.; Velankar, S. *J. Rheol.* **2011**, *55* (4), 713−731.
(30) Huitric, J.; Ville, J.; Médéric, P.; Moan, M.; Aubry, T. *J. Rheol.* **2009**, *53*, 1101−1119.
(31) Labaume, I.; Mederic, P.; Huitric, J.; Aubry, T. *J. Rheol.* **2013**, *57*, 377−392.
(32) Hyun, K.; Wilhelm, M.; O. Klein, C.; Cho, K. S.; Nam, J. G.; Ahn, K. H.; Lee, S. J.; Ewoldt, R. H.; McKinley, G. H. *Prog. Polym. Sci.* **2011**, *36*, 1697−1753.
(33) Wilhelm, M.; Maring, D.; Spiess, H. W. *Rheol. Acta* **1998**, *37* (4), 399−405.
(34) Wilhelm, M.; Reinheimer, P.; Ortseifer, M. *Rheol. Acta* **1999**, *38* (4), 349−356.
(35) Wilhelm, M.; Reinheimer, P.; Ortseifer, M.; Neidhöfer, T.; Spiess, H. W. *Rheol. Acta* **2000**, *39* (3), 241−246.
(36) Lim, H. T.; Ahn, K. H.; Hong, J. S.; Hyun, K. *J. Rheol.* **2013**, *57*, 767−789.
(37) Hyun, K.; Ahn, K. H.; Lee, S. J.; Sugimoto, M.; Koyama, K. *Rheol. Acta* **2006**, *46*, 123−129.
(38) Neidhofer, T.; Sioula, S.; Hadjichristidis, N.; Wilhelm, M. *Macromol. Rapid Commun.* **2004**, *25*, 1921−1926.
(39) Vittorias, I.; Parkinson, M.; Klimke, K.; Debbaut, B.; Wilhelm, M. *Rheol. Acta* **2007**, *46*, 321−340.
(40) Carotenuto, C.; Grosso, M.; Maffettone, P. L. *Macromolecules* **2008**, *41*, 4492−4500.
(41) Salehiyan, R.; Hyun, K. *Korean J. Chem. Eng.* **2013**, 1−10.
(42) Hyun, K.; Wilhelm, M. *Macromolecules* **2009**, *42* (1), 411−422.
(43) Wu, G.; Asai, S.; Sumita, M.; Hattori, T.; Higuchi, R.; Washiyama, J. *Colloid Polym. Sci.* **2000**, *278*, 220−228.
(44) Sundararaj, U.; Macosko, C. W. *Macromolecules* **1995**, *28* (8), 2647−2657.
(45) Elias, L.; Fenouillot, F.; Majesté, J. C.; Alcouffe, P.; Cassagnau, P. *Polymer* **2008**, *49*, 4378−4385.
(46) Cho, K. S.; Park, G. W. *J. Rheol.* **2013**, *57* (2), 647−678.
(47) Grosso, M.; Maffettone, P. L. *J. Non-Newtonian Fluid Mech.* **2007**, *143*, 48−58.
(48) Reinheimer, K.; Grosso, M.; Wilhelm, M. *J. Colloid Interface Sci.* **2011**, *360*, 818−825.